Biomaterials 31 (2010) 5143–5150

Contents lists available at ScienceDirect

Biomaterials

journal homepage: www.elsevier.com/locate/biomaterials

Nuclear morphology and deformation in engineered cardiac myocytes and tissues

Mark-Anthony P. Bray, William J. Adams, Nicholas A. Geisse, Adam W. Feinberg, Sean P. Sheehy, Kevin K. Parker*

Disease Biophysics Group, Harvard Stem Cell Institute, Wyss Institute for Biologically Inspired Engineering, School of Engineering and Applied Sciences, Harvard University, 29 Oxford St (Rm 322A), Cambridge, MA 02138, United States

ARTICLE INFO

Article history:
Received 2 March 2010
Accepted 9 March 2010
Available online 10 April 2010

Keywords:
Cardiac myocyte
Nucleus
Cytoskeleton
Myofibril
Extracellular matrix
Tissue engineering

ABSTRACT

Cardiac tissue engineering requires finely-tuned manipulation of the extracellular matrix (ECM) microenvironment to optimize internal myocardial organization. The myocyte nucleus is mechanically connected to the cell membrane via cytoskeletal elements, making it a target for the cellular response to perturbation of the ECM. However, the role of ECM spatial configuration and myocyte shape on nuclear location and morphology is unknown. In this study, printed ECM proteins were used to configure the geometry of cultured neonatal rat ventricular myocytes. Engineered one- and two-dimensional tissue constructs and single myocyte islands were assayed using live fluorescence imaging to examine nuclear position, morphology and motion as a function of the imposed ECM geometry during diastolic relaxation and systolic contraction. Image analysis showed that anisotropic tissue constructs cultured on micro-fabricated ECM lines possessed a high degree of nuclear alignment similar to that found *in vivo*; nuclei in isotropic tissues were polymorphic in shape with an apparently random orientation. Nuclear eccentricity was also increased for the anisotropic tissues, suggesting that intracellular forces deform the nucleus as the cell is spatially confined. During systole, nuclei experienced increasing spatial confinement in magnitude and direction of displacement as tissue anisotropy increased, yielding anisotropic deformation. Thus, the nature of nuclear displacement and deformation during systole appears to rely on a combination of the passive myofibril spatial organization and the active stress fields induced by contraction. Such findings have implications in understanding the genomic consequences and functional response of cardiac myocytes to their ECM surroundings under conditions of disease.

1. Introduction

Mechanical forces encode information at the cellular level that potentiates the activation, or suppression, of cell signaling pathways. The cytoskeleton is both an attenuator and propagator of this information, mediating bidirectional signaling between the extra- and intracellular spaces. In the heart, abnormal wall stresses are well known to prompt fibrosis and myocyte remodeling [1–3], suggesting that the myocyte grows and reorganizes its cytoskeleton to better accommodate its role in processing this information. Interestingly, these morphological changes are associated with alterations in the dimensions of the nucleus [4–7]. Research suggests that mechanically-stressed cardiac myocytes suffer nuclear envelope damage [8], which has been shown to produce alterations in gene transcription/translation in fibroblasts [9]. Therefore, the role of the nucleus in the cardiac mechanotransductive pathway is significant in light of the relationship between cell morphology and contractility.

The nucleus forms a focal point for mechanical signals originating from the extracellular space, permitting communication of the nucleus with the myocyte microenvironment. Previous studies have reported that endothelial cells and chondrocytes undergoing externally imposed stretch or compression [10–13], cellular contraction and spreading [14,15], or direct mechanical manipulation of integrin receptors [16] will experience concomitant nuclear deformation. Stresses transmitted from the extracellular matrix (ECM) by integrins are borne by an interconnected network of cytoskeleton (CSK) elements, some of which terminate on the nucleus [16–18]. In striated muscle, the intermediate filaments (IFs) interwoven in the sarcomeric Z-lines form a mechano-transductive conduit coupling myocyte shape to nuclear shape [19] which may play a role in genetic regulation during hypertrophy [20]. Previous studies have shown that spatially constraining the ECM environment (and thereby the cell shape) induces a corresponding CSK rearrangement, thereby modulating the internal stress distribution [21]. However, the effect of cardiac myocyte

* Corresponding author. Tel.: +1 617 495 2850; fax: +1 617 495 9837.
E-mail address: kkparker@seas.harvard.edu (K.K. Parker).

0142-9612/$ – see front matter © 2010 Elsevier Ltd. All rights reserved.
doi:10.1016/j.biomaterials.2010.03.028

shape on nuclear morphology as a function of the spatial cues presented by the surrounding ECM has yet to be examined.

The production of custom-designed extracellular substrates using photolithographic micropatterning (μCP) techniques is a versatile means of controlling cell shape and function [21–25]. The goal of this study is to examine the nuclear morphology and motion in engineered cardiac myocytes in three forms: single rectangular myocytes, multicellular one-dimensional strands and two-dimensional sheets. We quantify the nuclear morphology as a function of the myocyte shape and associated CSK architecture during: (1) Diastole (*i.e.*, resting state), where an intrinsic internal stress field in equilibrium is present and (2) Systole (*i.e.*, contraction), where an additional transient internal stress is created independently of any externally imposed forces.

2. Materials and methods

2.1. Myocyte culture

All animals were treated according to the *Guide of the Care and Use of Laboratory Animals* published by the US National Institutes of Health (NIH Publication No. 85-23, revised 1996). Cell cultures of neonatal rat ventricular myocytes were prepared from two-day old Sprague–Dawley rats. The isolated tissue was homogenized and washed in HBSS and then digested with trypsin and collagenase 14 h at 4 °C with agitation. Isolated myocytes were re-suspended in M199 culture medium supplemented with 10% heat-inactivated Fetal Bovine Serum, 10 mM HEPES, 20 mM glucose, 2 mM L-glutamine, 1.5 μM vitamin B-12, and 50 U/ml penicillin at 37 °C and agitated. Immediately after purification, myocytes were plated on 25 mm diameter PDMS-coated glass coverslips prepared as detailed above and kept in culture at 37 °C with a 5% CO_2 atmosphere. Medium was changed 24 h after plating to remove unattached and dead myocytes and every 48 h afterwards. 100 mM 5-bromo-2-deoxyuridine (BrdU) was added to the culture medium to prevent multiple nucleation.

2.2. Microcontact printing

Soft photolithographic techniques were used to create templates for μCP of the ECM protein fibronectin (FN). To produce patterned single myocytes for study, μCP designs consisting of rectangular shapes with a constant surface area of 2500 μm^2 were used to create patterned isolated islands of FN. Since studies have reported a range of myocyte length-to-width changes in diseased hearts, a variety of aspect ratios were created for the rectangular shapes: 1:1 (50×50 μm), 2:1 (70.7×35.4 μm), 3:1 (86.6×28.9 μm), and 7:1 (132.3×18.9 μm). After stamping the FN onto PDMS-coated coverslips, the coverslips were blocked with 1% Pluronic F127 (BASF, Mount Olive, NJ) to restrict myocyte adhesion to the FN islands.

To produce confluent myocyte tissue constructs, μCP was used to create FN patterns on polymer-coated coverslips consisting of 10 μm lines separated by 10 μm spaces and 20 μm lines separated by 20 μm spaces. These 2-D constructs are hereafter referred to as 10×10 μm and 20×20 μm tissue constructs, respectively. The coverslips were then coated with a reduced concentration of FN after stamping to create engineered tissue constructs of variable anisotropy. Isotropic tissue constructs were created by using stamps with no μCP features, producing a uniform FN distribution. One-dimensional strands of myocytes were created by treating the 10×10 μm lines with 1% Pluronic F127 instead of low concentration FN in order to prohibit cell adhesion between the FN lines.

2.3. Fluorescence recording and image acquisition

Coverslips containing myocytes patterned into confluent tissues, isolated strands or 2500 μm^2 myocytes were used for experiments three to four days after culture. Live myocytes were stained with 37.5 μM of the nucleic acid-sensitive dye 4′,6′-diamindino-2-phenylindole (DAPI) (Molecular Probes, OR) and incubated for 15 min. For the rectangular myocyte preparations, 20 μM of the membrane-selective dye di-8-ANEPPS was added in addition to the DAPI solution. The coverslip was then mounted in a custom heated bath and superfused continuously in warmed ($T = 35–37$ °C) oxygenated Tyrode's solution (in mmol/L: 135 NaCl, 5.4 KCl, 1.8 CaCl2, 1 MgCl2, 0.33 NaH2PO4, 5 HEPES, 5 glucose). The patterned tissue and strands were stimulated with a unipolar platinum point electrode at 1.5 times the capture threshold with a pulse width of 5 ms and a frequency of 3 Hz (MyoPacer stimulator, IonOptix, Milton, MA). For the rectangular myocyte preparations, 0.2 μM of epinephrine was added to the Tyrode's perfusate in order stimulate spontaneous contraction.

The patterned myocytes were visualized with a Cascade 512B CCD camera (Roper Scientific) mounted on an inverted microscope (DM 6000B, Leica Microsystems, Germany); the full system was mounted on a vibration-free table. A 63× objective (HCX Plan APO, NA 1.4, Leica) was used for fluorescence recording. Recordings were performed with a filter set with a bandpass excitation filter (450–490 nm), dichroic mirror (500 nm) and a bandpass emission filter (500–550 nm). Fluorescence was recorded in a full-frame format of 512×512 pixels (corresponding to 130×130 μm^2) at 28.58 fps for the tissue and strand construct preparations.

2.4. Immunocytochemistry

Engineered cardiac tissues and single myocytes were fixed in a solution consisting of 4% paraformaldehyde and 0.01% Triton X-100 in PBS buffer at 37 °C for 15 min and equilibrated to room temperature during incubation. All myocytes were stained with DAPI for chromatin, FITC-phalloidin for F-actin (Alexa 488 Phalloidin, Molecular Probes) and monoclonal mouse sarcomeric anti-α-actinin (EA-53; Sigma–Aldrich). The myocytes were then incubated for 1 h with secondary Alexa Fluor 594 conjugated goat anti-mouse IgG (β-tubulin, sarcomeric α-actinin) at a dilution of 1:200 (Molecular Probes). The fixed and stained patterned myocytes were visualized with a CCD camera (CoolSnap Photometrics, Roper Scientific) mounted on the same system as described above in a format of 1392×1040 pixels (corresponding to 142.68×106.60 μm^2).

3. Data analysis

Extensive discussion of data analysis methods is available in the Supplemental Material.

3.1. Extraction of nuclear parameters

The contour of the nucleus was extracted from the fluorescence image via thresholding. The nuclear perimeter pixels were used as input into an ellipse fitting algorithm [26] and was repeated for all detected nuclei in each image, permitting observation of the key elliptical parameters (centroid, major and minor axis length, eccentricity, perimeter, area and orientation). Eccentricity (e) is a measure of the shape of an ellipse and is in the range of [0,1]; a circle has an eccentricity of 0, and a more elongated shape is associated with a higher value of e.

For a time-lapse fluorescence image sequence, each frame was analyzed to observe the changes in the elliptical parameters as a function of time. Only those nuclei that could be accurately followed for the full duration of the image sequence were subjected to post-processing analysis. Each elliptical parameter was temporally smoothed by Savitzky–Golay filtering with a 5th-order polynomial, which rejects noise while maintaining necessary high-frequency components. The temporal evolution of the parameters was then divided into two phases: diastolic (non-contracting) and systolic (contracting) using K-means cluster analysis.

For the cardiac tissue and strand constructs, only those nuclei which were intact and in-focus were used. For rectangular myocytes, data was obtained only from those μCP FN islands containing a single, mononucleated myocyte.

3.2. Geometric considerations for rectangular myocyte data

In addition to observation of the nucleus via DAPI fluorescence, the outline of the rectangular cells was delineated for each set of data using the di-8-ANEPPS membrane stain. In this way, the nuclear parameters may be precisely registered with the associated myocyte shape.

In order to analyze and interpret the data in light of the inter-myocyte variation of parameters for a given shape, the data must be transformed to a uniform coordinate system. The registration procedure is as follows: The four corners of the cells are manually selected. A rectangle is then fit to the four points using non-linear optimization. The coordinate system is then (a) translated such that center is located at the origin, (b) rotated such that the long edges are parallel to the y-axis, and (c) scaled to match the specified μCP aspect ratio. Since the rectangle can be divided into four identical quadrants, the associated elliptical parameters for any given nucleus may be mapped into one quadrant through a series of

reflections around the *x* and *y* axes. All angles are measured with respect to the *x* axis.

3.3. Determination of cytoskeletal and nuclear alignment

To quantify the nuclear alignment in the two-dimensional tissue constructs, the mean cytoskeletal orientation (θ_{CSK}) was first calculated from the actin immunofluorescence images using a modified ridge detection algorithm [27,28]. We define nuclear alignment as the standard deviation of the differences between θ_{CSK} and the angular orientations of the individual nuclei, θ_{nucl} *i.e.*, STD ($\theta_{CSK} - \theta_{nucl}$); complete alignment of the nuclei with the global cytoskeletal orientation would therefore result in a value of zero.

Because the cytoskeletal orientation could not be determined from immunofluorescence in live tissue, the tissue orientation was inferred indirectly by applying the ridge detection algorithm on the DIC images of the tissue. The output of the algorithm provided the orientation of the tissue based on the optical images of the membrane (θ_{memb}). As in the diastolic measurements, the distribution was compiled from the difference between θ_{nucl} at systole and θ_{memb}.

3.4. Statistical analysis

All Cartesian statistical measures (*i.e.*, major/minor axis length, centroid location, and eccentricity) and associated changes are given as a mean ± standard deviation. Angular statistical measurements, such as orientation, are evaluated according to a circular distribution as follows [29]:

(1) The circular mean $\overline{\theta}$(in degrees) of a set of angles $\theta_1,\ldots\theta_n$, is evaluated by calculating

$$X = \frac{1}{n}\sum_{i=1}^{n}\cos\theta_i, \quad Y = \frac{1}{n}\sum_{i=1}^{n}\sin\theta_i \quad R = \sqrt{X^2+Y^2} \tag{1}$$

to which $\overline{\theta}$ is the solution to the equations

$$X = R\cos\overline{\theta}, \quad Y = R\sin\overline{\theta} \tag{2}$$

(2) The circular standard deviation (in degrees) is calculated as:

$$\sigma = \frac{180^\circ}{\pi}\sqrt{-2\ln R} \tag{3}$$

using *R* as given in (1).

Statistical significance was determined using one-way ANOVA, followed by Scheffé's multiple comparison test to determine differences. $P < 0.05$ was considered significant.

4. Results

4.1. Rectangular μCP cardiac cells

Fig. 1A–D illustrates the differences in cellular morphology when myocytes are cultured on rectangular 2500 μm^2 μCP FN islands. The cytoskeletal orientation of the myocytes reflects the aspect ratio of the underlying FN substrate: as the aspect ratio increases, the arrangement transitions from a myofibril pattern radiating towards the corners of the myocyte to one where the myofibrils preferentially parallel to the long axis of the myocyte.

The grouped nuclear measurements for the rectangular cells are shown in Fig. 2. As the cellular anisotropy increases, the nuclei are increasingly aligned with respect to the cellular longitudinal axis (Fig. 2A). This change in orientation is concomitant with nuclear morphology, with the major nuclear axes increasing in length (Fig. 2B); however, the minor axis length is not appreciably altered. While the nuclear cross-sectional area is not statistically different between the μCP myocytes (Fig. 2C), the eccentricity reflects the change in axes lengths, with the nuclei becoming more elongated as the cellular aspect ratio increases (Fig. 2D). Therefore, the reconfiguring of the actin cytoskeleton in response to the anisotropic ECM spatial cues has the effect of orienting and elongating the nucleus with respect to the longitudinal myocyte axis.

4.2. Engineered one- and two-dimensional cardiac tissues

4.2.1. Diastolic morphology

Fig. 1F–G illustrates the differences in cellular morphology and nuclear alignment when myocytes are cultured on μCP FN

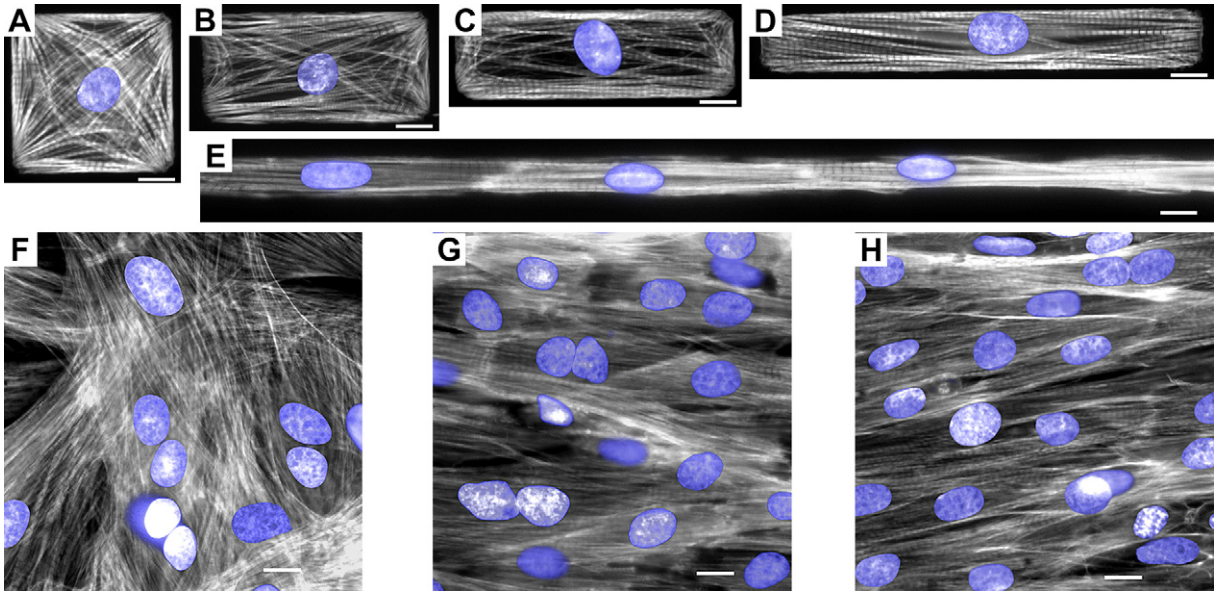

Fig. 1. Examples of μCP engineered single myocyte (A–D), fibers (E) and two-dimensional tissue (F–G) constructs. (A) 1:1; (B) 2:1; (C) 3:1; (D) 7:1; (E) Aligned fibers on a 20 μm FN line (F) Isotropic 2-D tissue construct; (G) Anisotropic 2-D tissue construct: 20 μm lines with 20 μm spacing; (H) Anisotropic 2-D tissue construct: 10 μm lines with 10 μm spacing. Actin is shown in gray with the DAPI stained nucleus highlighted and superimposed in blue. All panels to scale; scale bar: 10 μm.

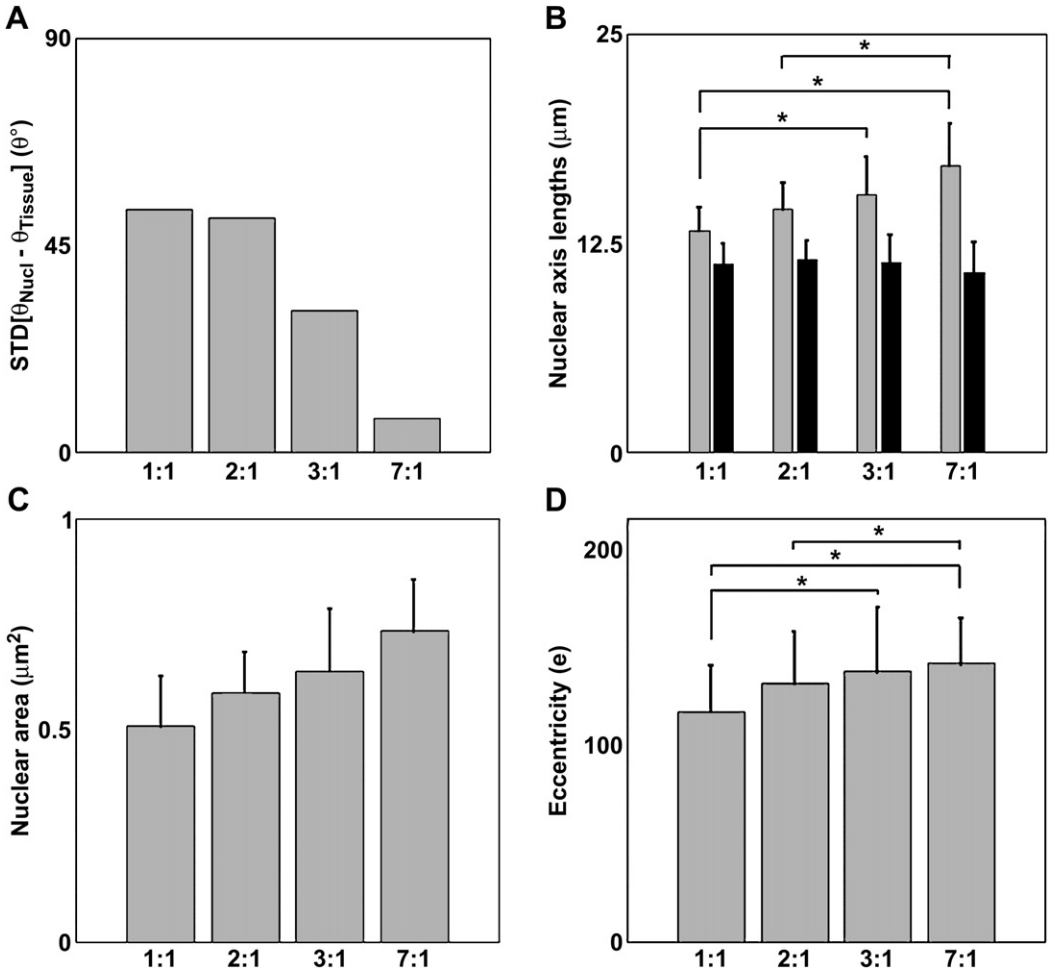

Fig. 2. Histograms of nuclear alignment and morphology in mononucleated μCP single myocytes: 1:1 ($n = 24$), 2:1 ($n = 30$), 3:1 ($n = 12$) and 7:1 ($n = 11$). (A) Alignment. (B) Major and minor axes lengths. (C) Cross-sectional area. (D) Eccentricity. Bars are given as mean ± standard deviation. Asterisk indicates statistical significance ($P < 0.05$).

substrates. Cells plated on the FN lines preferentially oriented their sarcomeres (visible as striated gaps within the actin stains) to the direction of the FN lines (Fig. 1G, H). In contrast, the cells cultured on a uniform FN distribution are polymorphic in shape with an irregular orientation in the absence of ECM spatial topography (Fig. 1F). Qualitatively, the nuclear alignment in the tissue constructs reflects the tissue orientation.

The nuclear alignment is shown as a function of tissue anisotropy in Fig. 3A. The difference in nuclear alignment between the 10×10 and 20×20 μm tissues was not statistically significant. However, the nuclear alignment of both anisotropic tissues was statistically different from that of the isotropic tissue, with the isotropic tissue possessing the largest angular deviation. This observation is consistent with the lack of cytoskeletal guidance provided by the ECM in the isotropic tissues.

The morphology of the nuclei in the tissue constructs was quantified by examining the nuclear axes lengths, cross-sectional area, and elliptical eccentricity. Fig. 3B shows that, similar to the nuclear alignment results, the mean minor axis lengths of both anisotropic tissues were statistically smaller than those of the isotropic tissues examined, with no statistical difference between the minor axis lengths of the anisotropic tissues. In contrast, the major axis lengths for all three tissue types were statistically similar. The influence of these parameters on the nuclear morphology is shown in Fig. 3C and D, highlighting that the nuclei in the anisotropic tissue possess a higher eccentricity (*i.e.*, are more elongated) and are smaller in mean cross-sectional area than their isotropic counterparts. Interestingly, as anisotropy increased, the minor axis decreased in the tissue constructs while the major axis increased in the μCP cells, but both changes resulted in a net increase in eccentricity as noted above.

In summary, the spatial cues induced by the linear ECM geometry produces cytoskeletal anisotropy in cultured myocytes with a corresponding elongation and alignment of the nucleus with the cytoskeleton while simultaneously decreasing the cross-sectional nuclear area.

4.2.2. Systolic morphology and motion

Live cellular imaging with a nuclear stain was used to observe the dynamic morphology of the nucleus as a function of time in the cardiac contraction cycle, with the parameters measured shown schematically in Fig. 4A. Fig. 4B shows the distribution of in-plane (*i.e.*, x–y) displacements of the nuclei in the engineered tissue, measured as the difference between the nuclear centroid locations at diastole and peak systole. The standard deviation of the displacements decreased with increasing anisotropy, indicating that nuclei experience an increasing amount of spatial confinement as tissue anisotropy is increased. Interestingly, the 1-D strands possessed a larger degree of nuclear displacements than the 2-D tissue constructs.

Fig. 4C shows the angular distribution of nuclei displacement with respect to the tissue orientation. In the 1-D strands (first

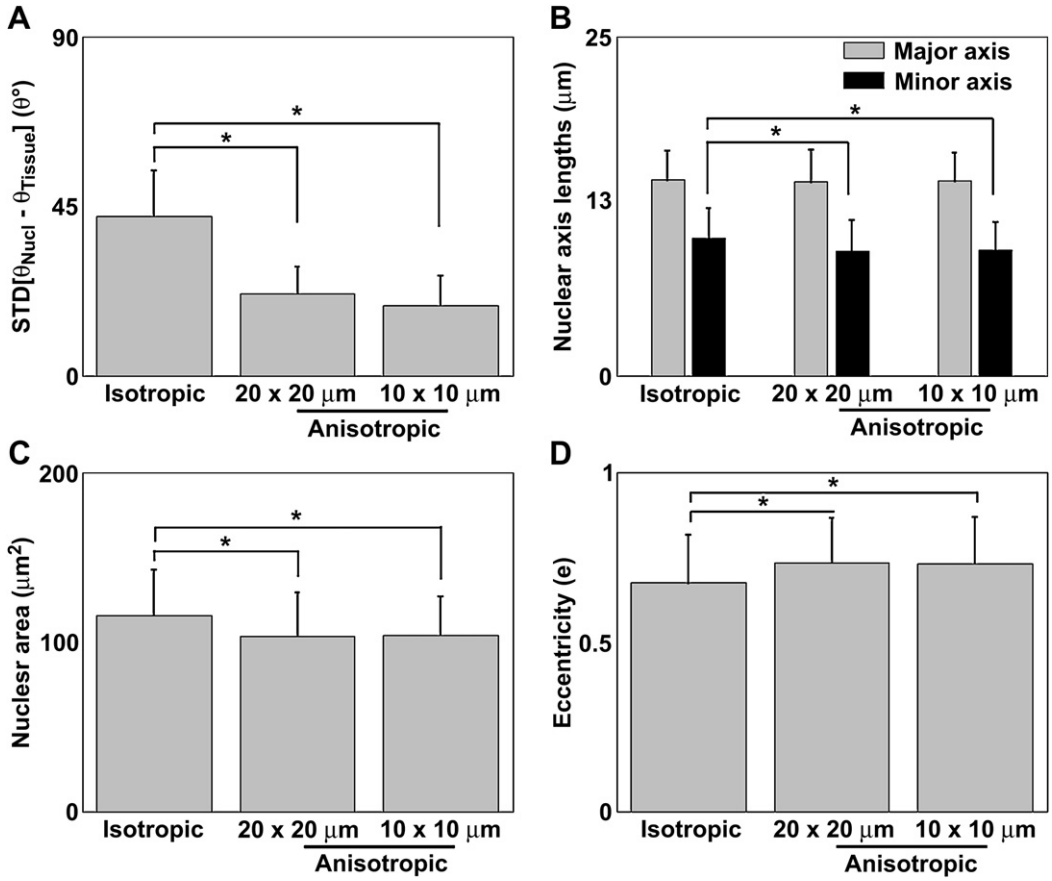

Fig. 3. Histograms of nuclear alignment and morphology in engineered cardiac tissue constructs. Three tissue types are shown: anisotropic tissue constructs created from μCP patterns with 10 mm lines with 10 μm spacing ($n = 1485$, left), 20 μm lines with 20 mm spacing ($n = 1507$, middle) and isotropic tissue constructs ($n = 842$, right). (A) Alignment. (B) Major and minor axes lengths. (C) Cross-sectional area. (D) Eccentricity. Bars are given as mean ± standard deviation. Asterisk indicates statistical significance ($P < 0.05$).

column), the direction of nuclei motion is correlated to the tissue orientation, with an unimodal distribution. However, the angular spread around the mode is fairly wide, in agreement with Fig. 4B. For isotropic tissue, the nuclei motion is not strongly correlated to the tissue orientation, and hence has a more uniform angular distribution with no discernable mode (second column). In contrast, the nuclear motion for the anisotropic tissue (third and fourth columns) is more unimodal, polarized towards 0°, indicating that the nuclear displacement during systole is aligned along the tissue orientation.

The change in nuclear morphology was also observed as a function of time for each of the engineered tissue constructs. Fig. 4D shows the relative proportion of changes in the major and minor nuclear axes length during systole. In the 1-D strands, the majority of the nuclei experienced lengthening of the major axes. For all 2-D tissue types, the greatest proportion of systolic nuclei experienced lengthening of the major axis and contraction of the minor axis. However, the remaining nuclei in the 1-D and 2-D tissues experienced other combinations of axial lengthening and shortening. These observations of systolic tissue indicate that tissue anisotropy confines both the magnitude and the direction of nuclear displacement as well as producing an anisotropic deformation of the nucleus during the cardiac contraction cycle.

5. Discussion

The specific means by which abnormal mechanical stresses are coupled to pathological gene expression remains largely unclear. However, it is known that the CSK is a mechanical mediator between the extracellular microenvironment and the intracellular sub-compartments. The ECM provides structural integrity and support for the heart at the cellular and organ levels. Therefore, changes in ECM distribution and geometry are capable of producing altered tissue stress patterns which can contribute to myocardial pathogenesis [30] and may impair the application of tissue engineering as a therapeutic response [31]. Coupled to abnormal changes in tissue stress is modification of gene expression patterns (*e.g.*, adult α-myosin and embryonic β-myosin [32]; sarcoplasmic reticulum Ca^{2+}-ATPase and phospholamban [33]). Additionally, if the integrity of the nuclear membrane is compromised, defective nuclear mechanics may also have downstream genetic effects [34]. The CSK acts as a mechanical link between the nuclear envelope and the cell membrane, and CSK-nuclear connections have been hypothesized to activate genes under hypertrophic conditions (such as the desmin-lamin network [19,20]). Hence, not only are spatial changes in the configuration of the ECM microenvironment are expected to alter the physiology of the cardiac myocyte, but these changes are also expected to be mediated (at least in part) via the mechanical connections between the CSK and the nucleus. In this study, microcontact printing techniques were used to provide cultured myocytes with custom-designed ECM geometries. Combined with nuclear staining of live myocytes, the resultant changes in nuclear morphology and motion permitted evaluation of the forces imposed on the nucleus due to ECM spatial cues reminiscent of normal and pathological myocardium. The effect of cell boundary shape on CSK organization has been investigated previously, primarily in fibroblasts. In particular, the imposition of corners on cellular geometry has revealed their emergent role as

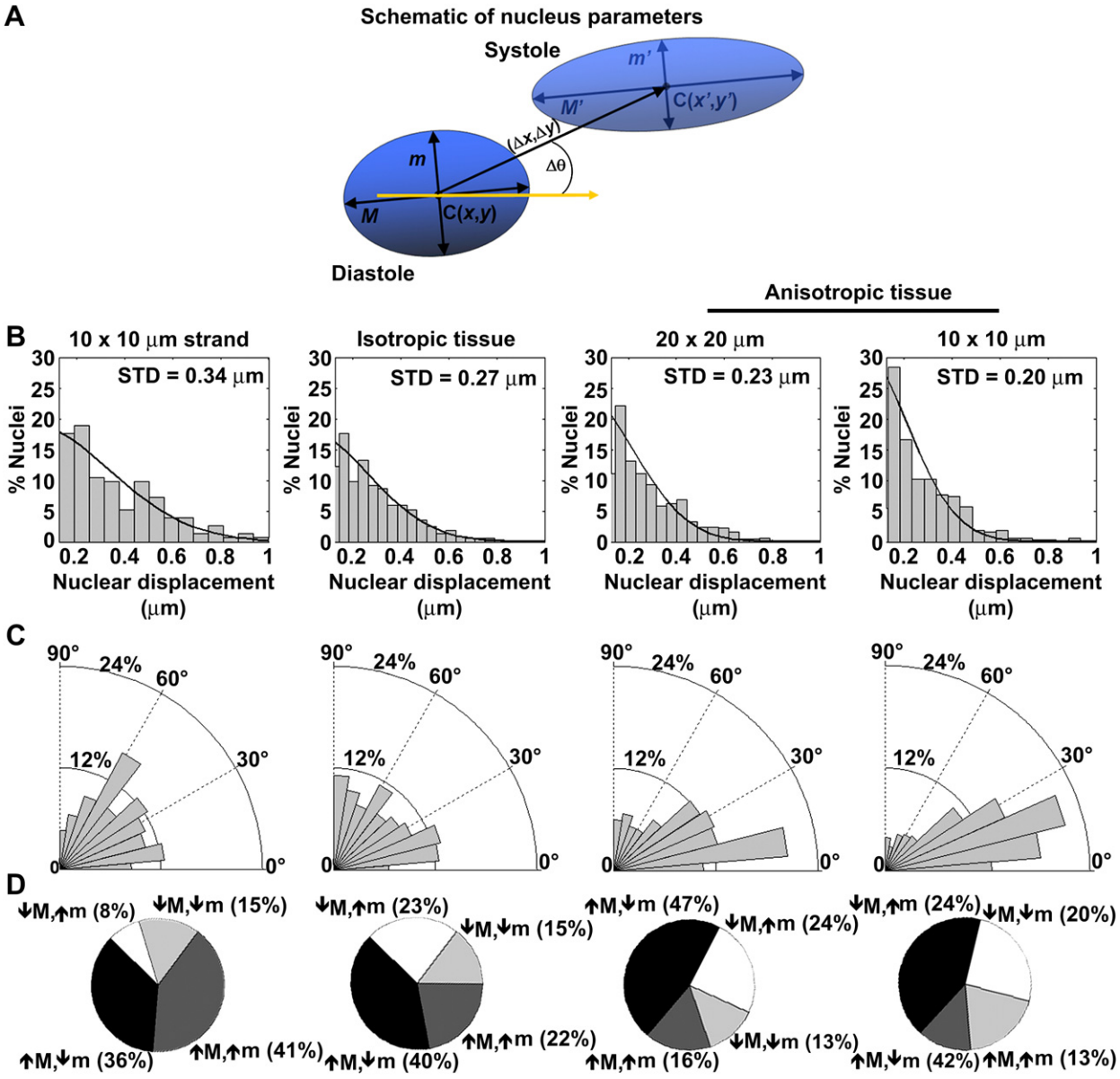

Fig. 4. Changes in nuclear location and morphology during contraction. *Top panel:* Schematic of nuclear parameters. Nucleus with diastolic centroid location C(x,y), major axis length M and minor axis length m is displaced (Δx,Δy) at an angle $\Delta\theta$ with respect to the tissue orientation (yellow arrow) to systolic location C(x',y') with a systolic morphology of major and minor axis lengths M' and m', respectively. *Lower panels:* Graphs of (A) magnitude and (B) direction of nuclear centroid displacement during systole with respect to tissue orientation, and (C) systolic changes in major and minor axis length, for 20×20 μm strands, isotropic tissue constructs, and 20×20 μm and 10×10 μm anisotropic tissue constructs. (A) Black line: Fitted normal distribution curve, with standard deviation indicated in the graph. (B): 0° and ±180° is parallel to tissue orientation. (C): Up-arrows (↑) and down-arrows (↓) indicate increase and decrease in axis length, respectively.

foci of lamellipodia extension, focal adhesion formation and tractional force generation [21,35,36]. However, while the dynamic linkage between the nucleus and cell periphery has been studied, the influence of specific peripheral geometries on transmission of the forces to the nucleus has not been a subject of examination.

Our study concerned itself with examining nuclei in cardiac cells and tissues spatially constrained by patterned ECM protein. Our results showing that nuclear alignment is closely correlated with tissue alignment are consistent with previous studies of cardiac myocytes on substrates containing linear microfabricated features, as well as a similar nuclear eccentricity [37]. However, our results suggest that topographical substrate complexity is not necessary to achieve a degree of control of nuclear alignment. A previous study has shown that the nuclei of transplanted adult myocytes have a rounded morphology, similar to that of cells located in infarcted tissue [38], which remained even after the transplanted cell orientation gradually conformed to that of the host cells. The isotropic tissue in our studies possessed a more rounded shape (*i.e.*, lower eccentricity) than that of the anisotropic tissue designed to replicate *in vivo* myocyte morphology (Fig. 3D). Therefore, the isotropic engineered tissue created by a uniform ECM distribution may provide a model system to assay nuclear changes in transplanted and infracted tissue. As shown in Fig. 3D, the nuclei in the anisotropic tissues are more elongated than those in the isotropic tissue; however, the nuclear area in the anisotropic tissue is also smaller. Assuming that the myocyte nuclei are approximately the same volume regardless of μCP protocol, this result may suggest that the additional spatial confinement imposed by the FN lines may cause the nuclei to extend further in the third spatial dimension (*i.e.*, z-direction).

While the nuclear morphology obtained from immunostaining provides insight into passive forces applied to the nucleus, it is a "snapshot" of the cytoskeletal mechanical coupling to the nucleus. By applying nuclear staining on contracting myocytes combined with dynamic nuclear tracking, this study permitted direct comparison of nuclei morphology and motion in the diastolic versus the systolic state. Our observations illustrated that the nucleus undergoes dynamic deformation during contraction, consistent with prior results demonstrating nuclear membrane deformation produced by mechanical connections to the shortening sarcomeres [39,40]. Furthermore, the nuclei in contracting cells returned to their original size and shape after the deformation induced by contraction, indicating that the nucleus acts like an elastic material within the normal range of stresses induced by contraction. Additional examination of the DAPI image sequences obtained from contracting myocytes revealed that the cross-sectional area of the nuclei was not conserved between diastole and systole. Three physical explanations for this observation are possible: (1) The nucleus may move in the optical axis (z-direction) during systole, presenting an adjacent cross-section with a different area in the field-of-view (FOV); (2) the nuclear cross-section is maintained in the FOV but the volume may expand or contract due to fluid influx/efflux; or (3) assuming the nucleus is volume-conserved, the nuclear cross-section is maintained in the FOV but the nucleus may either bulge or flatten in the z-direction. In regards to option (1), no out-of-plane changes in the nuclear granulation patterns were observed during DAPI imaging that would indicate a significant displacement in the z-axis. The nuclear volume loss or gain associated with (2) has been observed in chondrocytes undergoing compression [13,41], but the time scale of nuclear loading in these studies is much greater than that of the present one (hours or days as compared to seconds). Concerning (3), a similar anisotropic deformation response has been observed in tendon nuclei undergoing tensile strain [42] and chondrocyte and fibroblast nuclei undergoing compression [13,43]. However, this assumes that the nucleus does not undergo in-plane rotation around the long axis.

Several studies have used nuclear deformation as a metric to measure externally imposed strain on tissue [42,44,45]. On the single cell level, the observation of nuclear deformation in single cells has been previously used to examine large-scale forces transmitted through the cytoskeleton to the nucleus without direct observation of the cytoskeletal elements themselves [16,46]. In particular, manipulation of integrin proteins (which mediate forces from focal adhesion complexes) using magnetic beads indicated that forces of a physiologic range are capable of significantly deforming the nucleus as well [47]. The use of flexible substrata has proven to be useful in examining tractional forces applied to focal adhesion complexes [48,49]. These forces have been estimated to be on the same order of magnitude as the forces simultaneously transmitted to the nucleus [46]. However, studies of adhesion forces via flexible substrata have only recently been applied to cardiac myocytes, and without the benefit of μCP to control for cell shape [50]. Given the physiological importance of cardiac myocyte shape as a marker of tissue and cellular health or pathology, our study indicates that μCP combined with force measurements on flexible substrata to examine the magnitude of force transmitted to the nucleus during contraction would be a promising avenue of investigation.

6. Conclusions

When neonatal rat ventricular myocytes are cultured on micropatterned surfaces individually or as a multicellular tissue, their cytoskeleton remodels to the printed boundary conditions. Subsequently, the nuclear shapes change so that in anisotropic tissues a high degree of nuclear alignment is found; nuclei in isotropic tissues were polymorphic in shape with an apparently random orientation. Nuclear eccentricity was also increased for the anisotropic tissues, suggesting that extracellular boundary conditions, cytoskeletal architecture, and intracellular forces deform the nucleus. These data are important, because nuclear shape may play a role in determining the genetic differences measured between different tissue architectures.

Acknowledgements

This work has been supported by the Nanoscale Science and Engineering Center of the National Science Foundation under NSF award numbers PHY-0117795, NIH grant 1 R01 HL079126-01A2 (K. K.P.) and an UNCF-Merck postdoctoral fellowship (M.A.B.) We are grateful to Dr. Ashkan Vaziri and Dr. Poling Kuo for helpful discussions and suggestions during manuscript preparation.

Appendix. Supplementary data

Supplementary data associated with this article can be found in the on-line version, at doi:10.1016/j.biomaterials.2010.03.028.

References

[1] Grossman W, Jones D, McLaurin LP. Wall stress and patterns of hypertrophy in the human left ventricle. J Clin Investig 1975;56(1):56–64.
[2] Smith SH, Bishop SP. Regional myocyte size in compensated right ventricular hypertrophy in the ferret. J Mol Cell Cardiol 1985;17(10):1005–11.
[3] Gerdes AM, Campbell SE, Hilbelink DR. Structural remodeling of cardiac myocytes in rats with arteriovenous fistulas. Lab Investig 1988;59(6):857–61.
[4] Kostin S, Hein S, Arnon E, Scholz D, Schaper J. The cytoskeleton and related proteins in the human failing heart. Heart Fail Rev 2000;5(3):271–80.
[5] Cluzeaud F, Perennec J, de Amoral E, Willemin M, Hatt PY. Myocardial cell nucleus in cardiac overloading in the rat. Eur Heart J 1984;5(Suppl. F):271–80.
[6] Yan SM, Finato N, Di Loreto C, Beltrami CA. Nuclear size of myocardial cells in end-stage cardiomyopathies. Anal Quant Cytol Histol 1999;21(2):174–80.
[7] Gerdes AM, Liu Z, Zimmer HG. Changes in nuclear size of cardiac myocytes during the development and progression of hypertrophy in rats. Cardioscience 1994;5(3):203–8.
[8] Nikolova V, Leimena C, McMahon AC, Tan JC, Chandar S, Jogia D, et al. Defects in nuclear structure and function promote dilated cardiomyopathy in lamin A/C-deficient mice. J Clin Investig 2004;113(3):357–69.
[9] Lammerding J, Schulze PC, Takahashi T, Kozlov S, Sullivan T, Kamm RD, et al. Lamin A/C deficiency causes defective nuclear mechanics and mechanotransduction. J Clin Investig 2004;113(3):370–8.
[10] Caille N, Tardy Y, Meister JJ. Assessment of strain field in endothelial cells subjected to uniaxial deformation of their substrate. Ann Biomed Eng 1998;26(3):409–16.
[11] Caille N, Thoumine O, Tardy Y, Meister JJ. Contribution of the nucleus to the mechanical properties of endothelial cells. J Biomech 2002;35(2):177–87.
[12] Guilak F. Compression-induced changes in the shape and volume of the chondrocyte nucleus. J Biomech Eng 1995;28(12):1529–41.
[13] Knight MM, van de Breevaart Bravenboer J, Lee DA, van Osch GJVM, Weinans H, Bader DL. Cell and nucleus deformation in compressed chondrocyte-alginate constructs: temporal changes and calculation of cell modulus. Biochim Biophys Acta 2002;1570(1):1–8.
[14] Pienta KJ, Coffey DS. Nuclear-cytoskeletal interactions: evidence for physical connections between the nucleus and cell periphery and their alteration by transformation. J Cell Biochem 1992;49(4):357–65.
[15] Sims JR, Karp S, Ingber DE. Altering the cellular mechanical force balance results in integrated changes in cell, cytoskeletal and nuclear shape. J Cell Biol 1992;103(4):1215–22.
[16] Maniotis AJ, Chen CS, Ingber DE. Demonstration of mechanical connections between integrins, cytoskeletal filaments, and nucleoplasm that stabilize nuclear structure. Proc Natl Acad Sci U S A 1997;94(3):849–54.
[17] Ingber DE, Tensegrity I. Cell structure and hierarchical systems biology. J Cell Sci 2003;116(7):1157–73.
[18] Fey EG, Wan KM, Penman S. Epithelial cytoskeletal framework and nuclear matrix-intermediate filament scaffold: three-dimensional organization and protein composition. J Cell Biol 1984;98(6):1973–84.
[19] Lockard VG, Bloom S. Trans-cellular desmin-lamin B intermediate filament network in cardiac myocytes. J Mol Cell Cardiol 1993;25(3):303–9.
[20] Bloom S, Lockard VG, Bloom M. Intermediate filament-mediated stretch-induced changes in chromatin: a hypothesis for growth initiation in cardiac myocytes. J Mol Cell Cardiol 1996;28(10):2123–7.

[21] Parker KK, Brock AL, Brangwynne C, Mannix RJ, Wang N, Ostuni E, et al. Directional control of lamellipodia extension by constraining cell shape and orienting cell tractional forces. FASEB J 2002;16(10):1195–204.
[22] Singhvi R, Kumar A, Lopez GP, Stephanopoulos GN, Wang DI, Whitesides GM, et al. Engineering cell shape and function. Science 1994;264(5159):696–8.
[23] Lehnert D, Wehrle-Haller B, David C, Weiland U, Ballestrem C, Imhof BA, et al. Cell behaviour on micropatterned substrata: limits of extracellular matrix geometry for spreading and adhesion. J Cell Sci 2004;117(1):41–52.
[24] Huang S, Chen CS, Ingber DE. Control of cyclin D1, p27(Kip1), and cell cycle progression in human capillary endothelial cells by cell shape and cytoskeletal tension. Mol Biol Cell 1998;9(11):3179–93.
[25] Chen CS, Mrksich M, Huang S, Whitesides GM, Ingber DE. Geometric control of cell life and death. Science 1997;276(5317):1425–8.
[26] Fitzgibbon A, Pilu M, Fisher R. Direct least square fitting of ellipses. IEEE Trans Pattern Anal Mach Intell 1999;21(5):476–80.
[27] Hong L, Wan Y, Jain AK. Fingerprint image enhancement: algorithm and performance evaluation. IEEE Trans Pattern Anal Mach Intell 1998;20(8):777–89.
[28] Kovesi P. MATLAB and octave functions for computer vision and image processing [cited 2007/10/03/]; Available from: http://www.csse.uwa.edu.au/~pk/research/matlabfns/; 2005.
[29] Fisher NI. Statistical analysis of circular data. Cambridge: Cambridge University Press; 1993.
[30] Brower GL, Gardner JD, Forman MF, Murray DB, Voloshenyuk T, Levick SP, et al. The relationship between myocardial extracellular matrix remodeling and ventricular function. Eur J Cardiothorac Surg 2006;30(4):604–10.
[31] Furuta A, Miyoshi S, Itabashi Y, Shimizu T, Kira S, Hayakawa K, et al. Pulsatile cardiac tissue grafts using a novel three-dimensional cell sheet manipulation technique functionally integrates with the host heart, in vivo. Circ Res 2006;98(5):705–12.
[32] Tardiff JC, Hewett TE, Factor SM, Vikstrom KL, Robbins J, Leinwand LA. Expression of the β (slow)-isoform of MHC in the adult mouse heart causes dominant-negative functional effects. Am J Physiol Heart Circ Physiol 2000;278(2):H412–9.
[33] Matsui H, MacLennan DH, Alpert NR, Periasamy M. Sarcoplasmic reticulum gene expression in pressure overload-induced cardiac hypertrophy in rabbit. Am J Physiol Cell Physiol 1995;268(1):C252–8.
[34] Worman HJ, Courvalin JC. How do mutations in lamins A and C cause disease? J Clin Invest 2004;113(3):349–51.
[35] O'Neill CO, Jordan P, Riddle P, Ireland G. Narrow linear strips of adhesive substratum are powerful inducers of both growth and total focal contact area. J Cell Sci 1990;95(4):577–86.
[36] Brock A, Chang E, Ho CC, LeDuc P, Jiang X, Whitesides GM, et al. Geometric determinants of directional cell motility revealed using microcontact printing. Langmuir 2003;19(5):1611–7.
[37] Entcheva E, Bien H. Tension development and nuclear eccentricity in topographically controlled cardiac syncytium. Biomedical Microdevices 2003;5(2):163–8.
[38] Whittaker P, Müller-Ehmsen J, Dow JS, Kedes LH, Kloner RA. Development of abnormal tissue architecture in transplanted neonatal rat myocytes. Ann Thorac Surg 2003;75(5):1450–6.
[39] Franke WW. Attachment of muscle filaments to the outer membrane of the nuclear envelope. Zeitschrift für Zellforschung und mikroskopische Anatomie 1970;111(1):143–8.
[40] Bloom S. Structural changes in nuclear envelopes during elongation of heart muscle cells. J Cell Biol 1970;44(1):218–23.
[41] Buschmann MD, Hunziker EB, Kim YJ, Grodzinsky AJ. Altered aggrecan synthesis correlates with cell and nucleus structure in statically compressed cartilage. J Cell Sci 1996;109(2):499–508.
[42] Arnoczky SP, Lavagnino M, Whallon JH, Hoonjan A. In situ cell nucleus deformation in tendons under tensile load; a morphological analysis using confocal laser microscopy. J Orthop Res 2002;20(1):29–35.
[43] Houben F, Ramaekers FCS, Snoeckx LHEH, Broers JLV. Role of nuclear lamina-cytoskeleton interactions in the maintenance of cellular strength. Biochim Biophys Acta; 2006.
[44] Screen HR, Lee DA, Bader DL, Shelton JC. Development of a technique to determine strains in tendons using the cell nuclei. Biorheology 2003;40(1–3):361–8.
[45] Matyas J, Edwards P, Miniaci A, Shrive N, Wilson J, Bray R, et al. Ligament tension affects nuclear shape in situ: an in vitro study. Connect Tissue Res 1994;31(1):45–53.
[46] Jean RP, Gray DS, Spector AA, Chen CS. Characterization of the nuclear deformation caused by changes in endothelial cell shape. J Biomech Eng 2004;126(5):552–8.
[47] Hu S, Chen J, Butler JP, Wang N. Prestress mediates force propagation into the nucleus. Biochem Biophys Res Commun 2005;329(2):423–8.
[48] Beningo KA, Wang YL. Flexible substrata for the detection of cellular traction forces. Trends Cell Biol 2002;12(2):79–84.
[49] Wang N, Ostumi E, Whitesides GM, Ingber DE. Micropatterning tractional forces in living cells. Cell Motil Cytoskelet 2002;52(2):97–106.
[50] Balaban NQ, Schwarz US, Riveline D, Goichberg P, Tzur G, Sabanay I, et al. Force and focal adhesion assembly: a close relationship studied using elastic micropatterned substrates. Nat Cell Biol 2001;3(5):466–72.